

Stability of many-body localization in Kicked Ising model

Piotr Sierant,^{1,*} Maciej Lewenstein,^{1,2} Antonello Scardicchio,^{3,4} and Jakub Zakrzewski^{5,6}

¹*ICFO-Institut de Ciències Fotòniques, The Barcelona Institute of Science and Technology,
Av. Carl Friedrich Gauss 3, 08860 Castelldefels (Barcelona), Spain*

²*ICREA, Passeig Lluís Companys 23, 08010 Barcelona, Spain*

³*The Abdus Salam International Center for Theoretical Physics, Strada Costiera 11, 34151, Trieste, Italy*

⁴*INFN Sezione di Trieste, Via Valerio 2, 34127 Trieste, Italy*

⁵*Instytut Fizyki Teoretycznej, Uniwersytet Jagielloński, Lojasiewicza 11, PL-30-348 Kraków, Poland*

⁶*Mark Kac Complex Systems Research Center, Uniwersytet Jagielloński, Kraków, Poland*

(Dated: March 30, 2022)

We study many-body localization (MBL) transition in disordered Kicked Ising model using a polynomially filtered exact diagonalization (POLFED) algorithm. We quantitatively demonstrate that finite size effects at the MBL transition in disordered Kicked Ising model are less severe than in random field XXZ spin chains widely studied in the context of MBL. This allows us to observe consistent signatures of the transition to MBL phase for a several indicators of ergodicity breaking. We show that an assumption a power-law divergence of the correlation length at the MBL transition yields a critical exponent $\nu \approx 2$, consistent with the Harris criterion for 1D disordered systems.

Introduction. The eigenstate thermalization hypothesis [1–3] predicts that an isolated quantum system will reach an equilibrium determined only by a few macroscopic conserved quantities, independently of the details of the initial state. An exception to this ergodic paradigm is provided by a phenomenon of many-body localization (MBL) [4–10] which is a generic mechanism that inhibits the approach to equilibrium of interacting quantum many-body systems in the presence of disorder. This gives rise to a dynamical phase characterized by the emergence of local integrals of motion [11–15] that preserve the information about the initial state, resulting in a suppression of the transport [16, 17] and a slowdown of the entanglement spreading [18–20]. Numerical studies demonstrated that spin-1/2 XXZ chains [21–24], as well as bosonic models [25, 26] and systems of spinful fermions [27–31] undergo MBL at sufficiently strong disorder. Also periodically driven Floquet systems may become MBL [32–40] which allows to avoid heating [41] and enables exotic nonequilibrium phases of matter, such as time crystals [42–49] or Floquet insulators [50–54].

Recent investigations [55–60] of disordered many-body systems have unraveled, however, notorious difficulties in our understanding of the ergodic-to-MBL crossover. A nonmonotonic behavior of indicators of ergodicity breaking at the crossover and a limited range of system sizes (nowadays typically $L \sim 20$, restricted by the exponential growth of the Hilbert space) accessible in unbiased numerical approaches [61–64], do not allow for an unambiguous extrapolation of the numerical results for the typically considered spin-1/2 XXZ chains to the thermodynamic limit. Consequently, it remains unclear [65, 66] whether the numerically observed crossover between the ergodic and MBL regimes gives rise to a MBL phase that is stable in the thermodynamic limit [67–73] or whether the ergodicity is restored at length and time scales that increase with the disorder strength. Notably, constrained

spin chains follow the latter scenario and become ergodic in the thermodynamic limit [74] despite hosting a well-pronounced MBL regime at finite system sizes [75].

This demonstrates the need of identifying quantum many-body systems that allow for a clearer demonstration of MBL than for the widely studied spin-1/2 XXZ chains [76–107]. In this work we achieve this goal by performing large-scale numerical calculations for disordered Kicked Ising model (KIM) with state-of-the-art polynomially filtered exact diagonalization (POLFED) algorithm [62, 108]. We identify ergodic, critical and MBL regimes by considering system size dependent disorder strengths $W_X^T(L)$ and $W_X^*(L)$ and quantitatively demonstrate that finite size effects at the ergodic to MBL crossover in KIM are significantly weaker than in the XXZ model. This allows us to locate the MBL transition in KIM and investigate the scenario of a power-law divergence of correlation length at the transition.

The model. We consider a disordered KIM [109, 110] defined by the Floquet operator over one driving period for a 1D spin-1/2 chain

$$U_{\text{KIM}} = e^{-ig \sum_{j=1}^L \sigma_j^x} e^{-i \sum_{j=1}^L (J \sigma_j^z \sigma_{j+1}^z + h_j \sigma_j^z)}, \quad (1)$$

where $\sigma_j^{x,y,z}$ are Pauli operators, $h_j \in [0, 2\pi]$ are independent, uniformly distributed random variables and periodic boundary conditions are assumed. We take $g = J = 1/W$, so that W plays the role of the disorder strength in the system. The KIM is maximally ergodic for $W = 4/\pi$ [111–114]. Here, we consider higher values of W , up to a strong disorder limit in which $\sum_j h_j \sigma_j^z$ becomes a dominant term in U_{KIM} . To find the eigenvectors $|\psi_n\rangle$ and the corresponding eigenvalues $e^{i\phi_n}$ of U_{KIM} , we use the POLFED algorithm [62] employing a geometric sum filtering [108] (see [115] for details). This allows us to obtain eigenstates $|\psi_n\rangle$ for system sizes $L \leq 20$, significantly larger than for $L \leq 14$ considered in earlier exact diagonalization studies of KIM [36, 40].

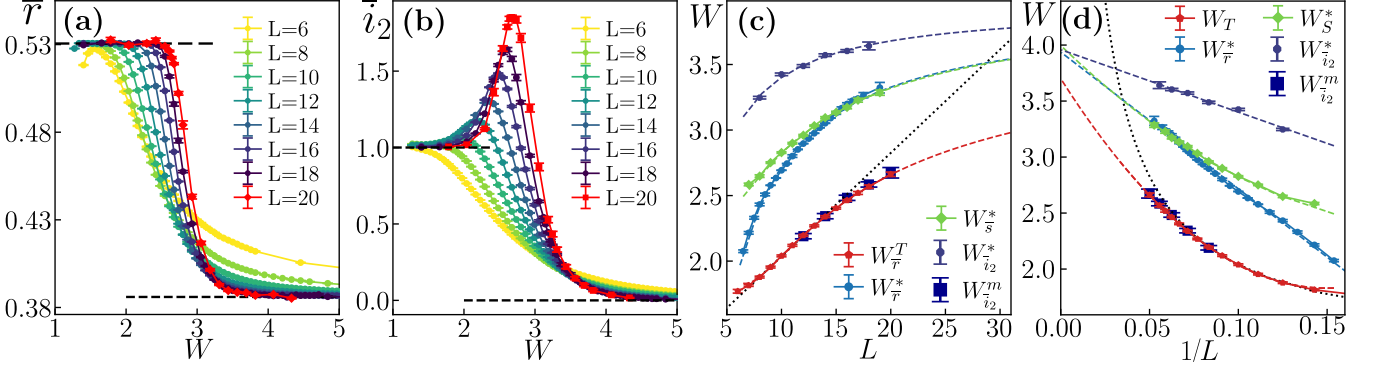


Figure 1. The ergodic-MLB crossover in KIM (1). Gap ratio \bar{r} (a) and rescaled QMI \bar{i}_2 (b) as function of disorder strength W for system size L ; dashed lines correspond to predictions for ergodic and MBL systems. Disorder strength $W_{\bar{r}}^T$ at which \bar{r} departs from the ergodic value and the crossing points W_X^* as function of L (c) and $1/L$ (d) where X is either the gap ratio \bar{r} , the rescaled entanglement entropy \bar{s} , or the rescaled QMI \bar{i}_2 ; the dotted lines denote $W_T(L) \sim L$ scaling; the dashed lines correspond to fits $W(L) = W_\infty + a/L + b/L^2$ with $W_\infty = 3.97 \pm 0.03$ for $W_{\bar{r}}^*(L)$, $W_{\bar{s}}^*(L)$ and $W_{\bar{i}_2}^*(L)$.

Ergodic-MLB crossover in KIM. We calculate $N_{\text{ev}} = \min\{2^L/10, 1000\}$ eigenvectors $|\psi_n\rangle$ of U_{KIM} . Due to the constant density of eigenphases ϕ_n , we can treat each eigenvector on equal footing. For concreteness, we choose eigenstates with eigenphases ϕ_n closest to $\phi_{\text{tg}} = 0$ and average results over more than $5 \cdot 10^4$, $5 \cdot 10^3$ and $5 \cdot 10^2$ disorder realizations, respectively for $L \leq 16$, $L = 17, 18$ and $L = 20$. To probe the properties of eigenphases, we compute the gap ratio $\bar{r} = \langle \min\{g_i, g_{i+1}\} \rangle / \max\{g_i, g_{i+1}\}$ where $g_i = \phi_{i+1} - \phi_i$ and $\langle \cdot \rangle$ denotes the average over the calculated fraction of spectrum and disorder realizations. For even L , we study the entanglement of eigenstates $|\psi_n\rangle$. The entanglement entropy [116] is given by $S(A) = -\sum_{i=1}^{i_M} \alpha_i^2 \log(\alpha_i^2)$, where $\alpha_{i+1} > \alpha_i$ are Schmidt basis coefficients [117] of the eigenstate $|\psi_n\rangle$ for a partition of the 1D lattice into a subsystem A and its complement. Choosing $A = [1, L/2]$, we calculate the rescaled entanglement entropy $\bar{s} = \langle S(A) \rangle / S_{\text{COE}}$ by taking the average $\langle \cdot \rangle$ over the eigenstates, disorder realizations and rescaling the result by average entanglement entropy S_{COE} of eigenstates of Circular Orthogonal Ensemble of random matrices (COE) that models the properties of U_{KIM} in the ergodic regime [118, 119]. For $A = [1, L/2]$ we also calculate the average Schmidt gap $\Delta = \langle \alpha_1^2 - \alpha_2^2 \rangle$. Furthermore, we calculate the quantum mutual information (QMI) $I_2 = S(B) + S(C) - S(B \cup C)$ for the subsystems $B = [1, \lceil L/4 \rceil]$, $C = (2 \lceil L/4 \rceil, 2 \lceil L/4 \rceil + \lfloor L/4 \rfloor]$ (where $\lceil \cdot \rceil$, $\lfloor \cdot \rfloor$ denote the ceil and floor functions), and obtain the rescaled QMI as $\bar{i}_2 = \langle I_2 \rangle / I_{\text{COE}}$ where I_{COE} is the average QMI for COE eigenstates. Also, we compute the spin stiffness $\bar{C} = \langle \sum_i \langle \psi_n | \sigma_i^z | \psi_n \rangle \rangle^2 / L$ which is an infinite time average of the spin-spin autocorrelation function $C(t) = \sum_i \text{Tr}[\sigma_i^z(t)\sigma_i^z(0)]/(L2^L)$.

As the strength of the disorder W increases, the gap ratio \bar{r} , shown in Fig. 1(a), decreases from $\bar{r} = \bar{r}_{\text{COE}} \approx 0.53$ characteristic for the ergodic regime to $\bar{r} = \bar{r}_{\text{PS}} \approx 0.386$ for an MBL system [120]. The QMI [121] measures the total amount of correlations between the subsystems B ,

C and decays exponentially with the distance between the subsystems in the MBL regime [122]. In the ergodic regime, the volume-law terms proportional to the lengths of subsystems B , C , $B \cup C$ cancel out and the QMI is equal to a system size independent value I_{COE} . Consequently, in Fig. 1(b), we observe a crossover in the rescaled QMI \bar{i}_2 as a function of W between the limiting values $\bar{i}_2 = 1$ and $\bar{i}_2 = 0$. The correlations between the subsystems are enhanced at the crossover, hence the rescaled QMI admits a maximum between the ergodic and MBL regimes. We observe the ergodic-MLB crossover also in the behavior of the rescaled entanglement entropy \bar{s} , Schmidt gap $\bar{\Delta}$, and spin stiffness \bar{C} , see [115].

To investigate the ergodic-MLB crossover we consider two system-size dependent disorder strengths: i) $W_X^T(L)$ – the disorder strength for which, at a given system size L , the quantity X is deviates by a small parameter p_X from its ergodic value; ii) $W_X^*(L)$ – the disorder strength for which the curves $X(W)$ cross for the system sizes $L - \Delta L$ and $L + \Delta L$ (where $\Delta L \ll L$). The disorder strengths $W_X^T(L)$ and $W_X^*(L)$ allow us to analyze the ergodic-MLB crossover in a quantitative fashion without resorting to any model of the transition. This is particularly advantageous in view of the recent controversies around the MBL transition [55–60, 69–73]. The disorder strength $W_X^T(L)$ may be considered as a boundary of the ergodic regime, whereas $W_X^*(L)$ provides an estimate of the critical disorder strength at given L . A regime between $W_X^T(L)$ and $W_X^*(L)$ is a critical region, vanishing for $L \rightarrow \infty$ if a transition between ergodic and MBL phases indeed occurs. For the disordered XXZ model, both disorder strengths increase monotonously with system size: $W_X^T(L) \sim L$ and $W_X^*(L) \sim W_C - \text{const}/L$ for $X = \bar{r}, \bar{s}$ [62]. The latter scaling suggests a finite critical disorder strength $W_C \approx 5.4$ (larger than $W_C \approx 3.7$ [24], but consistent with [82, 87]). However, the sealings of $W_X^T(L)$ and $W_X^*(L)$ are incompatible in the large system size limit, as $W_X^T(L)$ exceeds $W_X^*(L)$

at $L \leq L_0^{\text{XXZ}} \approx 50$ whereas $W_X^T(L) < W_X^*(L)$ by construction at any L . Therefore, when approaching the length scale L_0^{XXZ} (which appeared also in [71, 99]) one of the scalings must break down indicating either a presence of the MBL phase in the thermodynamic limit at $W > W_C$ (where $W_C \geq W_X^{T,*}(L)$) or showing the absence of the MBL phase (for example, when the linear increase of $W_X^T(L)$ prevails). However, the length scale L_0^{XXZ} is far beyond the reach of present day exact numerical calculations for the XXZ spin chain, which prevents one from unambiguously deciding which of the scenarios is realized in that model. Interestingly, numerical calculations for considerably larger system sizes of constrained spin chains suggest the second scenario: $W_X^T(L) \sim L$, $W_X^*(L) \sim L$ in which the extent of the ergodic regime increases indefinitely in the thermodynamic limit [74].

For the investigated KIM, we start by considering the gap ratio $X = \bar{r}$ and we set $p_{\bar{r}} = 0.01$, which yields $W_{\bar{r}}^T(L)$ shown in Fig. 1(c)-(d). We observe a linear scaling $W_{\bar{r}}^T(L) \sim L$ with system size L for $8 \leq L \leq 14$. Importantly, in contrast to the persistent linear drift of $W_{\bar{r}}^T(L) \sim L$ for XXZ spin chains, we see a clear deviation from the linear scaling for $L \geq 15$ for KIM. Therefore, the growth of $W_{\bar{r}}^T(L)$ with L is sublinear at sufficiently large system sizes, which is a first premise suggesting the stability of MBL in KIM in the $L \rightarrow \infty$ limit. Accessing system sizes $15 \leq L \leq 20$ with POLFED was necessary to uncover this premise for the MBL phase in KIM. The scaling of $W_{\bar{r}}^T(L)$ remains quantitatively the same for $0.002 < p_{\bar{r}} < 0.03$ and $W_{\bar{r}}^T(L)$ behaves analogously, see [115]. The disorder strength $W_{\bar{r}}^T(L)$ at which the gap ratio deviates from its ergodic value \bar{r}_{COE} coincides, to a good approximation, with the maximum $W_{\bar{i}_2}^m(L)$ of the rescaled QMI \bar{i}_2 which becomes pronounced at $L \leq 12$ (cf. Fig. 1(b)). The point $W_{\bar{i}_2}^m$ of the maximal correlations between subsystems B and C follows the linear scaling of $W_{\bar{r}}^T(L)$ for $L = 12, 14$ and deviates from it at $L \geq 16$.

Now, we turn to examination of the crossing point $W_X^*(L)$ in KIM. We use $|L_1 - L_2| \leq 2$ for $X = \bar{r}$, $|L_1 - L_2| = 2$ for $X = \bar{s}$ and $|L_1 - L_2| = 4$ for $X = \bar{i}_2$ and obtain $W_{\bar{r}}^*(L)$, $W_{\bar{s}}^*(L)$, $W_{\bar{i}_2}^*(L)$ shown in Fig. 1(c)-(d). The crossing points $W_{\bar{r}}^*(L)$ and $W_{\bar{s}}^*(L)$ differ at $L \lesssim 12$, but approach each other as the size of the system increases. Both $W_{\bar{r}}^*(L)$ and $W_{\bar{s}}^*(L)$ are well fitted by a second-order polynomial in $1/L$ whose extrapolation crosses with the extrapolation of the linear scaling of $W_{\bar{r}}^*(L)$ at $L_0^{\text{KIM}} \approx 28$. The length scale $L_0^{\text{KIM}} \approx 28$ is significantly smaller than the analogous length scale $L_0^{\text{XXZ}} \approx 50$ for XXZ spin chain. Therefore, the maximal system size investigated for KIM relative to this length scale, $L/L_0^{\text{KIM}} \approx 0.71$, is considerably larger than for the XXZ model $L/L_0^{\text{XXZ}} \approx 0.44$ [123]. This is the basis of a second premise that the ergodic-MBL crossover observed in KIM is stable in the large L limit. The crossing

points $W_{\bar{i}_2}^*(L)$ of the rescaled QMI \bar{i}_2 lies considerably above $W_{\bar{r}}^*(L)$, $W_{\bar{s}}^*(L)$. However, as shown in Fig. 1(d), $W_{\bar{i}_2}^*(L)$ is well fitted by a first order polynomial in $1/L$. Extrapolation of this polynomial to $L \rightarrow \infty$ limit gives a result consistent with extrapolations for $W_{\bar{r}}^*(L)$ and $W_{\bar{s}}^*(L)$, suggesting that the rescaled QMI \bar{i}_2 is subject to weaker finite size effects than \bar{r} or \bar{s} (cf. [124, 125]). Extrapolations yield an estimate of the critical disorder strength $W_\infty = 3.97 \pm 0.03$ [126].

The premises suggesting the presence of an MBL transition in KIM may be compared with features of the crossover between delocalized and localized regimes of Anderson model on random regular graphs (RRG) [127–129]. The crossover in the latter model shares similarities with the ergodic-MBL crossover [130]. Investigation of Anderson model on RRG of size $N = 2^L$ and varying connectivity [131] shows that: i) the boundary of the delocalized regime, $W_{\bar{r}}^T(L)$, follows a linear scaling with L that is replaced by a sublinear growth at $L \approx 13$; ii) the length scale at which the linear growth of $W_{\bar{r}}^T(L)$ crosses with the extrapolated scaling of the crossing point $W_{\bar{r}}^*(L)$ is $L_0^{\text{RRG}} \approx 25$; iii) extrapolation of the crossing point $W_{\bar{r}}^*(L)$ to $L \rightarrow \infty$ reproduces the exactly known critical disorder strength [132, 133]. All these observations are in line with the findings presented for U_{KIM} and support the interpretation of the results as indicating the presence of a transition to an MBL phase at the critical disorder strength $W_C \approx W_\infty$.

Finite-size scaling analysis. We now turn to finite-size scaling (FSS) analysis of the ergodic-MBL crossover in KIM. The MBL transition in XXZ spin chains was analyzed in the framework of power-law divergence of the correlation length [24, 134, 135] and of Kostelitz-Thouless-like scaling [99, 100, 136, 137] suggested by an avalanche mechanism of thermalization [138, 139]. Both scenarios were considered within the phenomenological renormalization group approaches [140–144]. Restricting the FSS to the vicinity of the critical disorder strength, which seems to be necessary, as exemplified by investigations of the 3D Anderson model [145], we cannot determine which of the scenarios of the MBL transition is realized in KIM. In the following, we assume the power-law divergence of the correlation length. Investigations of Anderson transition [146–150] suggest then the FSS ansatz:

$$X(W, L) = \psi_0(wL^{1/\nu}) + L^{-y}\psi_1(wL^{1/\nu}), \quad (2)$$

where X is the quantity analyzed, $w = (W - W_C)/W_C$ is the dimensionless distance from the critical point W_C , ν is the exponent describing the divergence of correlation length and the exponent y takes into account the corrections to the scaling due to irrelevant variables. We use the parametrization $\psi_1(wL^{1/\nu}) = a_0 + a_1 wL^{1/\nu}$, and consider the variable $X_m \equiv X - L^{-y}\psi_1(wL^{1/\nu})$ for which (2) implies the scaling form $X_m(W, L) = \psi_0(wL^{1/\nu})$ where ψ_0 is an unknown function. To achieve finite

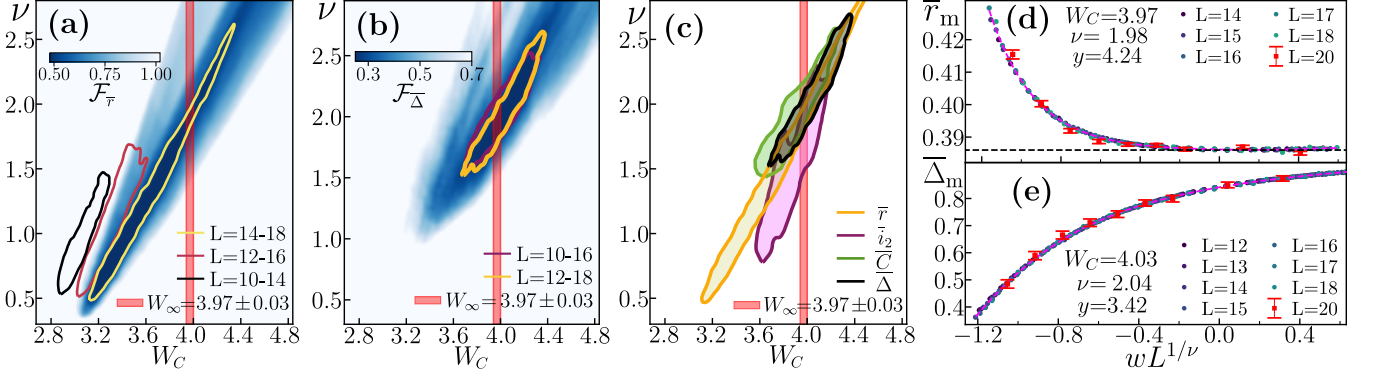


Figure 2. Finite size scaling analysis of ergodic-MBL crossover in KIM [1]. Cost functions $\mathcal{F}_{\bar{r}}$ (a) and $\mathcal{F}_{\bar{\Delta}}$ (b) are color coded for fixed ν , W_C , respectively for \bar{r} (system sizes considered in the collapse $L = 14-18$) and $\bar{\Delta}$ (for $L = 12-18$). The contours encompass ν , W_C for which \mathcal{F}_X is smaller than $\frac{4}{3}$ of its minimum \mathcal{F}_X^{\min} . (c): the contours $\mathcal{F}_X = \mu_X \mathcal{F}_X^{\min}$ for collapses of gap ratio \bar{r} ($L = 14-18$, for $\bar{r} \leq 0.43$), the Shmidt gap $\bar{\Delta}$ ($L = 12-18$, for $\bar{\Delta} \geq 0.44$), the rescaled QMI \bar{i}_2 ($L = 14-20$, for $\bar{i}_2 \leq 0.3$), the spin stiffness \bar{C} ($L = 12-18$, for $\bar{C} \geq 0.3$), $\mu_X = \frac{4}{3}$ for $X = \bar{r}, \bar{\Delta}, \bar{C}$ and $\mu_{\bar{i}_2} = 2$. Collapses for \bar{r}_m , $\bar{\Delta}_m$ shown in (d), (e).

size collapses of the data, we minimize a cost function $\mathcal{F}_X = \frac{\sum_j |X_{j+1}-X_j|}{\max\{X_j\}-\min\{X_j\}} - 1$ (with $X_j \equiv X_m(W_j, L_j)$ sorted according to the value of $wL^{1/\nu}$ [99]) by performing an optimization with respect to y , a_0 , a_1 and keeping $\nu \in [0.3, 3]$, $W_C \in [2.5, 5]$ fixed.

The collapses for the gap ratio $X = \bar{r}$ yield $\mathcal{F}_{\bar{r}}$ shown in Fig. 2(a). A wide minimum of $\mathcal{F}_{\bar{r}}$ in the direction $\nu \sim W_C$ shows that the FSS analysis alone is insufficient to determine the values of the critical parameters ν and W_C . Assuming additionally that $W_C \approx W_\infty = 3.97 \pm 0.03$, we find $\nu = 1.9 \pm 0.1$. The contours $\mathcal{F}_{\bar{r}} = \frac{4}{3} \mathcal{F}_{\bar{r}}^{\min}$, which encompass the broad minimum of the cost function, shift and elongate when the system sizes considered in the collapse increase from $L = 10-14$ to $L = 14-18$. This highlights the importance of finite size effects and it demonstrates qualitative changes in the behavior of \bar{r} when the system size is increased beyond $L = 14$. Analogous FSS analysis performed for the Schmidt gap $\bar{\Delta}$, finds a much better stability of the results with respect to the system size L , as exhibited by $\mathcal{F}_{\bar{\Delta}}$ presented in Fig. 2(b). A similar conclusion was obtained for the XXZ spin chain [87]. Despite the apparent correlation between ν and W_C , the minimum of $\mathcal{F}_{\bar{\Delta}}$ is narrower, consistent with $\nu = 2 \pm 0.5$ and $W_C = 4.1 \pm 0.5$. Assuming $W_C \approx W_\infty$, one gets $\nu = 1.95 \pm 0.1$. We perform similar collapses for the rescaled QMI \bar{i}_2 and the spin stiffness \bar{C} . The results, summarized in Fig. 2(c), display the correlation $\nu \sim W_C$ for all quantities considered. The intersection of all of the contours for $W_C \approx W_\infty$ yields $\nu = 2 \pm 0.1$ for which we obtain data collapses shown in Fig. 2(d),(e). Notably, we find that $\bar{r}_m \approx \bar{r}_{PS}$ at the MBL transition. See [115] for further details on the FSS analysis.

Conclusions and perspectives. We examined the ergodic-MBL crossover in disordered KIM by investigating the boundary of the ergodic regime $W_X^T(L)$ and the crossing point $W_X^*(L)$ that estimates the position a putative transition to MBL phase. The dependence of $W_X^T(L)$

and $W_X^*(L)$ on the system size L allows one to estimate a length scale L_0^{KIM} at which preasymptotic linear drifts at the ergodic-MBL crossover are replaced by an asymptotic critical behavior if the system undergoes a transition to an MBL phase in thermodynamic limit (if, instead, all features of the crossover start to drift linearly with L as L_0^{KIM} is approached, we may expect the MBL phase to be absent for $L \rightarrow \infty$, e.g. as in [74]). We found that $L_0^{\text{KIM}} \approx 28$ for KIM is considerably smaller than a corresponding length scale for disordered XXZ model $L_0^{\text{XXZ}} \approx 50$ [62]. This indicates that finite size effects at ergodic-MBL crossover in the former model are less severe than in the latter and allows us to observe signatures of transition to MBL phase along the whole ergodic-MBL crossover in KIM. A linear with L increase of $W_X^T(L)$ is replaced by a sub-linear growth at $L \geq 15$, consistent with a transition to MBL phase at sufficiently strong disorder. The crossing points $W_X^*(L)$ of gap ratio ($X = \bar{r}$), rescaled entanglement entropy ($X = \bar{s}$), rescaled QMI ($X = \bar{i}_2$) are well approximated by polynomials in $1/L$ which, upon extrapolation to $L \rightarrow \infty$ limit, consistently predict an ergodic-MBL transition in KIM at $W_C \approx 4$. We note that an analogous behavior of $W_X^T(L)$, $W_X^*(L)$ characterizes Anderson transition on random regular graphs, and that the extrapolation of $W_X^*(L)$ to $L \rightarrow \infty$ accurately predicts the position of the localization transition in that model [131]. Assuming a power-law divergence of the correlation length at the transition in KIM, we have shown that the estimated value of $W_C \approx 4$ is consistent with the correlation length exponent $\nu \approx 2$ fulfilling the Harris criterion [151–153].

Our results provide numerical arguments in favor of the presence of an MBL transition in a disordered 1D quantum many-body system system. This is of particular importance in view of the recent controversies around the MBL transition in the disordered XXZ spin chain. The latter model, in contrast to KIM, possesses $U(1)$ and time translation symmetries. Hence, our findings

support the intuition that the higher the symmetry of the model, the weaker the signatures of MBL (note that MBL does not occur in disordered spin chains with high $SU(2)$ symmetry [154]). Additionally, due to the lack of $U(1)$ symmetry, the arguments of [56, 59] against the stability of MBL do not apply to KIM. The demonstrated MBL in KIM provides an example of MBL in Floquet systems that underlies the stability of Floquet time crystals [46, 47, 49] and Floquet insulators [54] by providing a mechanism to completely eliminate the heating due to periodic driving of the system. do we acknowledge BSC as well??

Acknowledgments. PS acknowledges discussions with D. Luitz at the early stages of this work. PS and ML acknowledge ERC AdG NOQIA; Agencia Estatal de Investigación (R&D project CEX2019-000910-S, funded by MCIN/ AEI/10.13039/501100011033, Plan National FIDEUA PID2019-106901GB-I00, FPI, QUANTERA MAQS PCI2019-111828-2, Proyectos de I+D+I “Retos Colaboración” QUSPIN RTC2019-007196-7); Fundació Cellex; Fundació Mir-Puig; Generalitat de Catalunya through the European Social Fund FEDER and CERCA program (AGAUR Grant No. 2017 SGR 134, QuantumCAT U16-011424, co-funded by ERDF Operational Program of Catalonia 2014-2020); EU Horizon 2020 FET-OPEN OPTOlogic (Grant No 899794); National Science Centre, Poland (Symfonia Grant No. 2016/20/W/ST4/00314); European Union’s Horizon 2020 research and innovation programme under the Marie-Skłodowska-Curie grant agreement No 101029393 (STREDCH) and No 847648 (“La Caixa” Junior Leaders fellowships ID100010434: LCF/BQ/PI19/11690013, LCF/BQ/PI20/11760031, LCF/BQ/PR20/11770012, LCF/BQ/PR21/11840013). JZ is supported by the National Science Centre (Poland) under grant OPUS18 2019/35/B/ST2/00034. We acknowledge the support of PL-Grid Infrastructure.

-
- * Piotr.Sierant@icfo.eu
- [1] J. M. Deutsch, Quantum statistical mechanics in a closed system, *Phys. Rev. A* **43**, 2046 (1991).
 - [2] M. Srednicki, Chaos and quantum thermalization, *Phys. Rev. E* **50**, 888 (1994).
 - [3] L. D’Alessio, Y. Kafri, A. Polkovnikov, and M. Rigol, From quantum chaos and eigenstate thermalization to statistical mechanics and thermodynamics, *Advances in Physics* **65**, 239 (2016), <https://doi.org/10.1080/00018732.2016.1198134>.
 - [4] D. Basko, I. Aleiner, and B. Altshuler, Metal-insulator transition in a weakly interacting many-electron system with localized single-particle states, *Ann. Phys. (NY)* **321**, 1126 (2006).
 - [5] I. V. Gornyi, A. D. Mirlin, and D. G. Polyakov, Interacting electrons in disordered wires: Anderson localization and low- t transport, *Phys. Rev. Lett.* **95**, 206603 (2005).
 - [6] M. Žnidarič, T. Prosen, and P. Prelovšek, Many-body localization in the Heisenberg XXZ magnet in a random field, *Phys. Rev. B* **77**, 064426 (2008).
 - [7] A. Pal and D. A. Huse, Many-body localization phase transition, *Phys. Rev. B* **82**, 174411 (2010).
 - [8] R. Nandkishore and D. A. Huse, Many-body-localization and thermalization in quantum statistical mechanics, *Ann. Rev. Cond. Mat. Phys.* **6**, 15 (2015).
 - [9] F. Alet and N. Laflorencie, Many-body localization: An introduction and selected topics, *Comptes Rendus Physique* **19**, 498 (2018).
 - [10] D. A. Abanin, E. Altman, I. Bloch, and M. Serbyn, Colloquium: Many-body localization, thermalization, and entanglement, *Rev. Mod. Phys.* **91**, 021001 (2019).
 - [11] D. A. Huse, R. Nandkishore, and V. Oganesyan, Phenomenology of fully many-body-localized systems, *Phys. Rev. B* **90**, 174202 (2014).
 - [12] V. Ros, M. Mueller, and A. Scardicchio, Integrals of motion in the many-body localized phase, *Nuclear Physics B* **891**, 420 (2015).
 - [13] T. B. Wahl, A. Pal, and S. H. Simon, Efficient representation of fully many-body localized systems using tensor networks, *Phys. Rev. X* **7**, 021018 (2017).
 - [14] M. Mierzejewski, M. Kozarzewski, and P. Prelovšek, Counting local integrals of motion in disordered spinless-fermion and Hubbard chains, *Phys. Rev. B* **97**, 064204 (2018).
 - [15] S. J. Thomson and M. Schiró, Time evolution of many-body localized systems with the flow equation approach, *Phys. Rev. B* **97**, 060201 (2018).
 - [16] M. Žnidarič, A. Scardicchio, and V. K. Varma, Diffusive and subdiffusive spin transport in the ergodic phase of a many-body localizable system, *Phys. Rev. Lett.* **117**, 040601 (2016).
 - [17] B. Bertini, F. Heidrich-Meisner, C. Karrasch, T. Prosen, R. Steinigeweg, and M. Žnidarič, Finite-temperature transport in one-dimensional quantum lattice models, *Rev. Mod. Phys.* **93**, 025003 (2021).
 - [18] G. D. Chiara, S. Montangero, P. Calabrese, and R. Fazio, Entanglement entropy dynamics of heisenberg chains, *Journal of Statistical Mechanics: Theory and Experiment* **2006**, P03001 (2006).
 - [19] M. Serbyn, Z. Papić, and D. A. Abanin, Universal slow growth of entanglement in interacting strongly disordered systems, *Physical review letters* **110**, 260601 (2013).
 - [20] F. Iemini, A. Russomanno, D. Rossini, A. Scardicchio, and R. Fazio, Signatures of many-body localization in the dynamics of two-site entanglement, *Physical Review B* **94**, 214206 (2016).
 - [21] V. Oganesyan and D. A. Huse, Localization of interacting fermions at high temperature, *Phys. Rev. B* **75**, 155111 (2007).
 - [22] L. F. Santos, G. Rigolin, and C. O. Escobar, Entanglement versus chaos in disordered spin chains, *Phys. Rev. A* **69**, 042304 (2004).
 - [23] A. De Luca and A. Scardicchio, Ergodicity breaking in a model showing many-body localization, *EPL (Euro-physics Letters)* **101**, 37003 (2013).
 - [24] D. J. Luitz, N. Laflorencie, and F. Alet, Many-body localization edge in the random-field Heisenberg chain, *Phys. Rev. B* **91**, 081103 (2015).
 - [25] P. Sierant and J. Zakrzewski, Many-body localization of bosons in optical lattices, *New Journal of Physics* **20**,

- 043032 (2018).
- [26] T. Orell, A. A. Michailidis, M. Serbyn, and M. Silveri, Probing the many-body localization phase transition with superconducting circuits, *Phys. Rev. B* **100**, 134504 (2019).
- [27] R. Mondaini and M. Rigol, Many-body localization and thermalization in disordered Hubbard chains, *Phys. Rev. A* **92**, 041601 (2015).
- [28] P. Prelovšek, O. S. Barišić, and M. Žnidarič, Absence of full many-body localization in the disordered Hubbard chain, *Phys. Rev. B* **94**, 241104 (2016).
- [29] J. Zakrzewski and D. Delande, Spin-charge separation and many-body localization, *Phys. Rev. B* **98**, 014203 (2018).
- [30] M. Kozarzewski, P. Prelovšek, and M. Mierzejewski, Spin subdiffusion in the disordered Hubbard chain, *Phys. Rev. Lett.* **120**, 246602 (2018).
- [31] J. Richter and A. Pal, Many-body localization and delocalization dynamics in the thermodynamic limit, arXiv e-prints , arXiv:2202.10498 (2022), arXiv:2202.10498 [cond-mat.stat-mech].
- [32] A. Lazarides, A. Das, and R. Moessner, Fate of many-body localization under periodic driving, *Phys. Rev. Lett.* **115**, 030402 (2015).
- [33] P. Ponte, Z. Papić, F. m. c. Huvaneers, and D. A. Abanin, Many-body localization in periodically driven systems, *Phys. Rev. Lett.* **114**, 140401 (2015).
- [34] P. Ponte, A. Chandran, Z. Papić, and D. A. Abanin, Periodically driven ergodic and many-body localized quantum systems, *Annals of Physics* **353**, 196 (2015).
- [35] D. A. Abanin, W. De Roeck, and F. Huvaneers, Theory of many-body localization in periodically driven systems, *Annals of Physics* **372**, 1 (2016).
- [36] L. Zhang, V. Khemani, and D. A. Huse, A floquet model for the many-body localization transition, *Phys. Rev. B* **94**, 224202 (2016).
- [37] E. Bairey, G. Refael, and N. H. Lindner, Driving induced many-body localization, *Phys. Rev. B* **96**, 020201 (2017).
- [38] R. Sahay, F. Machado, B. Ye, C. R. Laumann, and N. Y. Yao, Emergent ergodicity at the transition between many-body localized phases, *Phys. Rev. Lett.* **126**, 100604 (2021).
- [39] S. J. Garratt and J. T. Chalker, Many-body delocalization as symmetry breaking, *Phys. Rev. Lett.* **127**, 026802 (2021).
- [40] M. Sonner, M. Serbyn, Z. Papić, and D. A. Abanin, Thouless energy across the many-body localization transition in floquet systems, *Phys. Rev. B* **104**, L081112 (2021).
- [41] R. Moessner and S. L. Sondhi, Equilibration and order in quantum floquet matter, *Nature Physics* **13**, 424 (2017).
- [42] K. Sacha, Modeling spontaneous breaking of time-translation symmetry, *Phys. Rev. A* **91**, 033617 (2015).
- [43] K. Sacha and J. Zakrzewski, Time crystals: a review, *Reports on Progress in Physics* **81**, 016401 (2017).
- [44] V. Khemani, A. Lazarides, R. Moessner, and S. L. Sondhi, Phase structure of driven quantum systems, *Phys. Rev. Lett.* **116**, 250401 (2016).
- [45] D. V. Else, B. Bauer, and C. Nayak, Floquet time crystals, *Phys. Rev. Lett.* **117**, 090402 (2016).
- [46] S. Choi, J. Choi, R. Landig, G. Kucsko, H. Zhou, J. Isoya, F. Jelezko, S. Onoda, H. Sumiya, V. Khemani, C. von Keyserlingk, N. Y. Yao, E. Demler, and M. D. Lukin, Observation of discrete time-crystalline order in a disordered dipolar many-body system, *Nature* **543**, 221 (2017).
- [47] P. Bordia, H. Lüschen, U. Schneider, M. Knap, and I. Bloch, Periodically driving a many-body localized quantum system, *Nature Physics* **13**, 460 (2017).
- [48] A. Pizzi, D. Malz, G. De Tomasi, J. Knolle, and A. Nunnenkamp, Time crystallinity and finite-size effects in clean floquet systems, *Phys. Rev. B* **102**, 214207 (2020).
- [49] X. Mi, M. Ippoliti, C. Quintana, A. Greene, Z. Chen, J. Gross, F. Arute, K. Arya, J. Atalaya, R. Babbush, J. C. Bardin, J. Basso, A. Bengtsson, A. Bilmes, A. Bourassa, L. Brill, M. Broughton, B. B. Buckley, D. A. Buell, B. Burkett, N. Bushnell, B. Chiaro, R. Collins, W. Courtney, D. Debroy, S. Demura, A. R. Derk, A. Dunsworth, D. Eppens, C. Erickson, E. Farhi, A. G. Fowler, B. Foxen, C. Gidney, M. Giustina, M. P. Harrigan, S. D. Harrington, J. Hilton, A. Ho, S. Hong, T. Huang, A. Huff, W. J. Huggins, L. B. Ioffe, S. V. Isakov, J. Iveland, E. Jeffrey, Z. Jiang, C. Jones, D. Kafri, T. Khattar, S. Kim, A. Kitaev, P. V. Klimov, A. N. Korotkov, F. Kostritsa, D. Landhuis, P. Laptev, J. Lee, K. Lee, A. Locharla, E. Lucero, O. Martin, J. R. McClean, T. McCourt, M. McEwen, K. C. Miao, M. Mohseni, S. Montazeri, W. Mruczkiewicz, O. Naaman, M. Neeley, C. Neill, M. Newman, M. Y. Niu, T. E. O'Brien, A. Opremcak, E. Ostby, B. Pato, A. Petukhov, N. C. Rubin, D. Sank, K. J. Satzinger, V. Shvarts, Y. Su, D. Strain, M. Szalay, M. D. Trevithick, B. Villalonga, T. White, Z. J. Yao, P. Yeh, J. Yoo, A. Zalcman, H. Neven, S. Boixo, V. Smelyanskiy, A. Megrant, J. Kelly, Y. Chen, S. L. Sondhi, R. Moessner, K. Kechedzhi, V. Khemani, and P. Roushan, Time-crystalline eigenstate order on a quantum processor, *Nature* **601**, 531 (2022).
- [50] H. C. Po, L. Fidkowski, T. Morimoto, A. C. Potter, and A. Vishwanath, Chiral floquet phases of many-body localized bosons, *Phys. Rev. X* **6**, 041070 (2016).
- [51] F. Nathan, D. Abanin, E. Berg, N. H. Lindner, and M. S. Rudner, Anomalous floquet insulators, *Phys. Rev. B* **99**, 195133 (2019).
- [52] R. Roy and F. Harper, Periodic table for floquet topological insulators, *Phys. Rev. B* **96**, 155118 (2017).
- [53] F. Harper and R. Roy, Floquet topological order in interacting systems of bosons and fermions, *Phys. Rev. Lett.* **118**, 115301 (2017).
- [54] M. S. Rudner and N. H. Lindner, Band structure engineering and non-equilibrium dynamics in floquet topological insulators, *Nature Reviews Physics* **2**, 229 (2020).
- [55] J. Šuntajs, J. Bonča, T. Prosen, and L. Vidmar, Quantum chaos challenges many-body localization, *Phys. Rev. E* **102**, 062144 (2020).
- [56] M. Kiefer-Emmanouilidis, R. Unanyan, M. Fleischhauer, and J. Sirker, Evidence for unbounded growth of the number entropy in many-body localized phases, *Phys. Rev. Lett.* **124**, 243601 (2020).
- [57] D. Sels and A. Polkovnikov, Dynamical obstruction to localization in a disordered spin chain, *Phys. Rev. E* **104**, 054105 (2021).
- [58] D. Sels and A. Polkovnikov, Thermalization of dilute impurities in one dimensional spin chains, arXiv e-prints , arXiv:2105.09348 (2021), arXiv:2105.09348 [quant-ph].
- [59] M. Kiefer-Emmanouilidis, R. Unanyan, M. Fleis-

- chhauer, and J. Sirker, Slow delocalization of particles in many-body localized phases, *Phys. Rev. B* **103**, 024203 (2021).
- [60] P. Sierant and J. Zakrzewski, Challenges to observation of many-body localization, arXiv e-prints, arXiv:2109.13608 (2021), [arXiv:2109.13608 \[cond-mat.dis-nn\]](#).
- [61] F. Pietracaprina, N. Macé, D. J. Luitz, and F. Alet, Shift-invert diagonalization of large many-body localizing spin chains, *SciPost Phys.* **5**, 45 (2018).
- [62] P. Sierant, M. Lewenstein, and J. Zakrzewski, Polynomially filtered exact diagonalization approach to many-body localization, *Phys. Rev. Lett.* **125**, 156601 (2020).
- [63] R. Van Beeumen, G. D. Kahanamoku-Meyer, N. Y. Yao, and C. Yang, A scalable matrix-free iterative eigensolver for studying many-body localization, in *Proceedings of the International Conference on High Performance Computing in Asia-Pacific Region* (2020) pp. 179–187.
- [64] T. Kutsuzawa and S. Todo, Nested Iterative Shift-invert Diagonalization for Many-body Localization in the Random-field Heisenberg Chain, arXiv e-prints, arXiv:2203.09732 (2022), [arXiv:2203.09732 \[cond-mat.dis-nn\]](#).
- [65] A. Morningstar, L. Colmenarez, V. Khemani, D. J. Luitz, and D. A. Huse, Avalanches and many-body resonances in many-body localized systems (2021), [arXiv:2107.05642 \[cond-mat.dis-nn\]](#).
- [66] D. Sels, Markovian baths and quantum avalanches (2021), [arXiv:2108.10796 \[cond-mat.dis-nn\]](#).
- [67] J. Z. Imbrie, Diagonalization and many-body localization for a disordered quantum spin chain, *Phys. Rev. Lett.* **117**, 027201 (2016).
- [68] J. Z. Imbrie, On many-body localization for quantum spin chains, *Journal of Statistical Physics* **163**, 998 (2016).
- [69] P. Sierant, D. Delande, and J. Zakrzewski, Thouless time analysis of anderson and many-body localization transitions, *Phys. Rev. Lett.* **124**, 186601 (2020).
- [70] D. Abanin, J. Bardarson, G. De Tomasi, S. Gopalakrishnan, V. Khemani, S. Parameswaran, F. Pollmann, A. Potter, M. Serbyn, and R. Vasseur, Distinguishing localization from chaos: Challenges in finite-size systems, *Annals of Physics* **427**, 168415 (2021).
- [71] R. K. Panda, A. Scardicchio, M. Schulz, S. R. Taylor, and M. Žnidarič, Can we study the many-body localisation transition?, *EPL (Europhysics Letters)* **128**, 67003 (2020).
- [72] P. J. D. Crowley and A. Chandran, A constructive theory of the numerically accessible many-body localized to thermal crossover (2021), [arXiv:2012.14393 \[cond-mat.dis-nn\]](#).
- [73] R. Ghosh and M. Žnidarič, Theory of growth of number entropy in disordered systems (2022), [arXiv:2112.12987 \[cond-mat.dis-nn\]](#).
- [74] P. Sierant, E. G. Lazo, M. Dalmonte, A. Scardicchio, and J. Zakrzewski, Constraint-induced delocalization, *Phys. Rev. Lett.* **127**, 126603 (2021).
- [75] C. Chen, F. Burnell, and A. Chandran, How does a locally constrained quantum system localize?, *Phys. Rev. Lett.* **121**, 085701 (2018).
- [76] D. J. Luitz, N. Laflorencie, and F. Alet, Extended slow dynamical regime close to the many-body localization transition, *Phys. Rev. B* **93**, 060201 (2016).
- [77] X. Yu, D. J. Luitz, and B. K. Clark, Bimodal entanglement entropy distribution in the many-body localization transition, *Phys. Rev. B* **94**, 184202 (2016).
- [78] T. C. Berkelbach and D. R. Reichman, Conductivity of disordered quantum lattice models at infinite temperature: Many-body localization, *Phys. Rev. B* **81**, 224429 (2010).
- [79] K. Agarwal, S. Gopalakrishnan, M. Knap, M. Müller, and E. Demler, Anomalous diffusion and griffiths effects near the many-body localization transition, *Phys. Rev. Lett.* **114**, 160401 (2015).
- [80] S. Bera, H. Schomerus, F. Heidrich-Meisner, and J. H. Bardarson, Many-body localization characterized from a one-particle perspective, *Phys. Rev. Lett.* **115**, 046603 (2015).
- [81] M. Serbyn, Z. Papić, and D. A. Abanin, Criterion for many-body localization-delocalization phase transition, *Phys. Rev. X* **5**, 041047 (2015).
- [82] T. Devakul and R. R. P. Singh, Early breakdown of area-law entanglement at the many-body delocalization transition, *Phys. Rev. Lett.* **115**, 187201 (2015).
- [83] C. L. Bertrand and A. M. García-García, Anomalous thouless energy and critical statistics on the metallic side of the many-body localization transition, *Phys. Rev. B* **94**, 144201 (2016).
- [84] T. Enss, F. Andraschko, and J. Sirker, Many-body localization in infinite chains, *Phys. Rev. B* **95**, 045121 (2017).
- [85] M. Serbyn, Z. Papić, and D. A. Abanin, Thouless energy and multifractality across the many-body localization transition, *Phys. Rev. B* **96**, 104201 (2017).
- [86] S. Bera, G. De Tomasi, F. Weiner, and F. Evers, Density propagator for many-body localization: Finite-size effects, transient subdiffusion, and exponential decay, *Phys. Rev. Lett.* **118**, 196801 (2017).
- [87] J. Gray, S. Bose, and A. Bayat, Many-body localization transition: Schmidt gap, entanglement length, and scaling, *Phys. Rev. B* **97**, 201105 (2018).
- [88] J. A. Kjäll, Many-body localization and level repulsion, *Phys. Rev. B* **97**, 035163 (2018).
- [89] E. V. H. Doggen, F. Schindler, K. S. Tikhonov, A. D. Mirlin, T. Neupert, D. G. Polyakov, and I. V. Gornyi, Many-body localization and delocalization in large quantum chains, *Phys. Rev. B* **98**, 174202 (2018).
- [90] N. Macé, F. Alet, and N. Laflorencie, Multifractal scalings across the many-body localization transition, *Phys. Rev. Lett.* **123**, 180601 (2019).
- [91] L. Herviou, S. Bera, and J. H. Bardarson, Multiscale entanglement clusters at the many-body localization phase transition, *Phys. Rev. B* **99**, 134205 (2019).
- [92] P. Sierant and J. Zakrzewski, Level statistics across the many-body localization transition, *Phys. Rev. B* **99**, 104205 (2019).
- [93] M. Schiulaz, E. J. Torres-Herrera, and L. F. Santos, Thouless and relaxation time scales in many-body quantum systems, *Phys. Rev. B* **99**, 174313 (2019).
- [94] L. A. Colmenarez, P. A. McClarty, M. Haque, and D. J. Luitz, Statistics of correlation functions in the random heisenberg chain, *SciPost Physics* **7**, 10.21468/scipostphys.7.5.064 (2019).
- [95] P. Huembeli, A. Dauphin, P. Wittek, and C. Gogolin, Automated discovery of characteristic features of phase transitions in many-body localization, *Phys. Rev. B* **99**, 104106 (2019).

- [96] T. Chanda, P. Sierant, and J. Zakrzewski, Many-body localization transition in large quantum spin chains: The mobility edge, *Phys. Rev. Research* **2**, 032045 (2020).
- [97] P. Sierant and J. Zakrzewski, Model of level statistics for disordered interacting quantum many-body systems, *Phys. Rev. B* **101**, 104201 (2020).
- [98] E. J. Torres-Herrera, G. De Tomasi, M. Schiulaz, F. Pérez-Bernal, and L. F. Santos, Self-averaging in many-body quantum systems out of equilibrium: Approach to the localized phase, *Phys. Rev. B* **102**, 094310 (2020).
- [99] J. Šuntajs, J. Bonča, T. Prosen, and L. Vidmar, Ergodicity breaking transition in finite disordered spin chains, *Phys. Rev. B* **102**, 064207 (2020).
- [100] N. Laflorencie, G. Lemarié, and N. Macé, Chain breaking and kosterlitz-thouless scaling at the many-body localization transition in the random-field heisenberg spin chain, *Phys. Rev. Research* **2**, 042033 (2020).
- [101] B. Villalonga and B. K. Clark, Eigenstates hybridize on all length scales at the many-body localization transition, arXiv e-prints , arXiv:2005.13558 (2020), arXiv:2005.13558 [cond-mat.dis-nn].
- [102] B. Villalonga and B. K. Clark, Characterizing the many-body localization transition through correlations, arXiv e-prints , arXiv:2007.06586 (2020), arXiv:2007.06586 [cond-mat.dis-nn].
- [103] L. Vidmar, B. Krajewski, J. Bonča, and M. Mierzejewski, Phenomenology of spectral functions in disordered spin chains at infinite temperature, *Phys. Rev. Lett.* **127**, 230603 (2021).
- [104] T. Szoldra, P. Sierant, K. Kottmann, M. Lewenstein, and J. Zakrzewski, Detecting ergodic bubbles at the crossover to many-body localization using neural networks, *Phys. Rev. B* **104**, L140202 (2021).
- [105] S. Nandy, F. Evers, and S. Bera, Dephasing in strongly disordered interacting quantum wires, *Phys. Rev. B* **103**, 085105 (2021).
- [106] F. Kotthoff, F. Pollmann, and G. De Tomasi, Distinguishing an Anderson insulator from a many-body localized phase through space-time snapshots with neural networks, *Phys. Rev. B* **104**, 224307 (2021), arXiv:2108.04244 [cond-mat.dis-nn].
- [107] K. Hémery, F. Pollmann, and A. Smith, Identifying correlation clusters in many-body localized systems, *Phys. Rev. B* **105**, 064202 (2022), arXiv:2108.03251 [cond-mat.dis-nn].
- [108] D. J. Luitz, Polynomial filter diagonalization of large Floquet unitary operators, *SciPost Phys.* **11**, 21 (2021).
- [109] T. Prosen, General relation between quantum ergodicity and fidelity of quantum dynamics, *Phys. Rev. E* **65**, 036208 (2002).
- [110] T. Prosen, Chaos and complexity of quantum motion, *Journal of Physics A: Mathematical and Theoretical* **40**, 7881 (2007).
- [111] M. Akila, D. Waltner, B. Gutkin, and T. Guhr, Particle-time duality in the kicked ising spin chain, *Journal of Physics A: Mathematical and Theoretical* **49**, 375101 (2016).
- [112] P. Kos, M. Ljubotina, and T. Prosen, Many-body quantum chaos: Analytic connection to random matrix theory, *Phys. Rev. X* **8**, 021062 (2018).
- [113] B. Bertini, P. Kos, and T. Prosen, Exact spectral form factor in a minimal model of many-body quantum chaos, *Phys. Rev. Lett.* **121**, 264101 (2018).
- [114] A. Lerose, M. Sonner, and D. A. Abanin, Influence matrix approach to many-body floquet dynamics, *Phys. Rev. X* **11**, 021040 (2021).
- [115] See Supplementary Material at [URL will be inserted by publisher] for details on POLFED diagonalization algorithm, gap ratio, quantum mutual information or average Schmidt gap analyses in the crossover between MBL and ergodic phases as well as additional arguments on finite size scaling. It includes Refs. [155–165].
- [116] L. Amico, R. Fazio, A. Osterloh, and V. Vedral, Entanglement in many-body systems, *Rev. Mod. Phys.* **80**, 517 (2008).
- [117] I. Bengtsson and K. Życzkowski, *Geometry of Quantum States: An Introduction to Quantum Entanglement* (Cambridge University Press, 2006).
- [118] L. D’Alessio and M. Rigol, Long-time behavior of isolated periodically driven interacting lattice systems, *Phys. Rev. X* **4**, 041048 (2014).
- [119] L. Vidmar and M. Rigol, Entanglement entropy of eigenstates of quantum chaotic hamiltonians, *Phys. Rev. Lett.* **119**, 220603 (2017).
- [120] Y. Y. Atas, E. Bogomolny, O. Giraud, and G. Roux, Distribution of the ratio of consecutive level spacings in random matrix ensembles, *Phys. Rev. Lett.* **110**, 084101 (2013).
- [121] B. Groisman, S. Popescu, and A. Winter, Quantum, classical, and total amount of correlations in a quantum state, *Phys. Rev. A* **72**, 032317 (2005).
- [122] G. De Tomasi, S. Bera, J. H. Bardarson, and F. Pollmann, Quantum mutual information as a probe for many-body localization, *Phys. Rev. Lett.* **118**, 016804 (2017).
- [123] We used $L = 22$ here, since the data for $L = 24, 26$ are statistically less significant due to small number of disorder realizations [61, 62].
- [124] A. Zabalo, M. J. Gullans, J. H. Wilson, S. Gopalakrishnan, D. A. Huse, and J. H. Pixley, Critical properties of the measurement-induced transition in random quantum circuits, *Phys. Rev. B* **101**, 060301 (2020).
- [125] P. Sierant and X. Turkeshi, Universal behavior beyond multifractality of wave-functions at measurement-induced phase transitions, arXiv e-prints , arXiv:2109.06882 (2021), arXiv:2109.06882 [cond-mat.stat-mech].
- [126] $\lim_{L \rightarrow \infty} W_r^T(L) \approx 3.7 < W_\infty$, but since W_r^T is the most distant point of the crossover from the critical point, we regard this value as a lower bound for the critical disorder strength.
- [127] R. Abou-Chakra, D. J. Thouless, and P. W. Anderson, *Journal of Physics C: Solid State Physics* **6**, 1734 (1973).
- [128] A. D. Mirlin and Y. V. Fyodorov, Localization transition in the anderson model on the bethe lattice: Spontaneous symmetry breaking and correlation functions, *Nuclear Physics B* **366**, 507 (1991).
- [129] F. Evers and A. D. Mirlin, Anderson transitions, *Rev. Mod. Phys.* **80**, 1355 (2008).
- [130] K. S. Tikhonov, A. D. Mirlin, and M. A. Skvortsov, Anderson localization and ergodicity on random regular graphs, *Phys. Rev. B* **94**, 220203 (2016).
- [131] P. Sierant, M. Lewenstein, and A. Scardicchio, in preparation.
- [132] G. Parisi, S. Pascazio, F. Pietracaprina, V. Ros, and A. Scardicchio, Anderson transition on the bethe lattice:

- an approach with real energies, *Journal of Physics A: Mathematical and Theoretical* **53**, 014003 (2019).
- [133] K. S. Tikhonov and A. D. Mirlin, Critical behavior at the localization transition on random regular graphs, *Phys. Rev. B* **99**, 214202 (2019).
- [134] J. A. Kjäll, J. H. Bardarson, and F. Pollmann, Many-body localization in a disordered quantum Ising chain, *Phys. Rev. Lett.* **113**, 107204 (2014).
- [135] V. Khemani, D. N. Sheng, and D. A. Huse, Two universality classes for the many-body localization transition, *Phys. Rev. Lett.* **119**, 075702 (2017).
- [136] M. Hopjan, G. Orso, and F. Heidrich-Meisner, [arXiv:2105.10584](#).
- [137] A. S. Aramthottil, T. Chanda, P. Sierant, and J. Zakrzewski, Finite-size scaling analysis of the many-body localization transition in quasiperiodic spin chains, *Phys. Rev. B* **104**, 214201 (2021).
- [138] W. De Roeck and F. m. c. Huvveneers, Stability and instability towards delocalization in many-body localization systems, *Phys. Rev. B* **95**, 155129 (2017).
- [139] D. J. Luitz, F. m. c. Huvveneers, and W. De Roeck, How a small quantum bath can thermalize long localized chains, *Phys. Rev. Lett.* **119**, 150602 (2017).
- [140] R. Vosk, D. A. Huse, and E. Altman, Theory of the many-body localization transition in one-dimensional systems, *Phys. Rev. X* **5**, 031032 (2015).
- [141] A. C. Potter, R. Vasseur, and S. A. Parameswaran, Universal properties of many-body delocalization transitions, *Phys. Rev. X* **5**, 031033 (2015).
- [142] A. Goremykina, R. Vasseur, and M. Serbyn, Analytically solvable renormalization group for the many-body localization transition, *Phys. Rev. Lett.* **122**, 040601 (2019).
- [143] P. T. Dumitrescu, A. Goremykina, S. A. Parameswaran, M. Serbyn, and R. Vasseur, Kosterlitz-thouless scaling at many-body localization phase transitions, *Phys. Rev. B* **99**, 094205 (2019).
- [144] A. Morningstar, D. A. Huse, and J. Z. Imbrie, Many-body localization near the critical point, *Phys. Rev. B* **102**, 125134 (2020).
- [145] J. Šuntajs, T. Prosen, and L. Vidmar, Spectral properties of three-dimensional anderson model, *Annals of Physics* **435**, 168469 (2021), special issue on Philip W. Anderson.
- [146] K. Slevin and T. Ohtsuki, Corrections to scaling at the anderson transition, *Phys. Rev. Lett.* **82**, 382 (1999).
- [147] Y. Ueoka and K. Slevin, Dimensional dependence of critical exponent of the anderson transition in the orthogonal universality class, *Journal of the Physical Society of Japan* **83**, 084711 (2014).
- [148] E. Tarquini, G. Birolì, and M. Tarzia, Critical properties of the anderson localization transition and the high-dimensional limit, *Phys. Rev. B* **95**, 094204 (2017).
- [149] K. Slevin and T. Ohtsuki, Critical exponent of the anderson transition using massively parallel supercomputing, *Journal of the Physical Society of Japan* **87**, 094703 (2018).
- [150] M. Pino, Scaling up the anderson transition in random-regular graphs, *Phys. Rev. Research* **2**, 042031 (2020).
- [151] A. B. Harris, Effect of random defects on the critical behaviour of ising models, *Journal of Physics C: Solid State Physics* **7**, 1671 (1974).
- [152] J. T. Chayes, L. Chayes, D. S. Fisher, and T. Spencer, Finite-size scaling and correlation lengths for disordered systems, *Phys. Rev. Lett.* **57**, 2999 (1986).
- [153] A. Chandran, C. R. Laumann, and V. Oganesyan, (2015), [arXiv:1509.04285](#).
- [154] I. V. Protopopov, R. K. Panda, T. Parolini, A. Scardicchio, E. Demler, and D. A. Abanin, Non-abelian symmetries and disorder: A broad nonergodic regime and anomalous thermalization, *Phys. Rev. X* **10**, 011025 (2020).
- [155] C. Lanczos, An iteration method for the solution of the eigenvalue problem of linear differential and integral operators1, *Journal of Research of the National Bureau of Standards* **45** (1950).
- [156] J. Cullum and W. E. Donath, A block lanczos algorithm for computing the q algebraically largest eigenvalues and a corresponding eigenspace of large, sparse, real symmetric matrices, in *1974 IEEE Conference on Decision and Control including the 13th Symposium on Adaptive Processes* (IEEE, 1974) pp. 505–509.
- [157] Y. Saad, On the rates of convergence of the lanczos and the block-lanczos methods, *SIAM Journal on Numerical Analysis* **17**, 687 (1980).
- [158] C. Bekas, E. Kokiopoulou, and Y. Saad, Computation of large invariant subspaces using polynomial filtered lanczos iterations with applications in density functional theory, *SIAM Journal on Matrix Analysis and Applications* **30**, 397 (2008).
- [159] H.-R. Fang and Y. Saad, A filtered lanczos procedure for extreme and interior eigenvalue problems, *SIAM Journal on Scientific Computing* **34**, A2220 (2012).
- [160] A. Pieper, M. Kreutzer, A. Alvermann, M. Galgon, H. Fehske, G. Hager, B. Lang, and G. Wellein, High-performance implementation of chebyshev filter diagonalization for interior eigenvalue computations, *Journal of Computational Physics* **325**, 226 (2016).
- [161] H. Guan and W. Zhang, Dual applications of Chebyshev polynomials method: Efficientlyfinding thousands of central eigenvalues for many-spin systems, *SciPost Phys.* **11**, 103 (2021).
- [162] Fino and Algazi, Unified matrix treatment of the fast walsh-hadamard transform, *IEEE Transactions on Computers* **C-25**, 1142 (1976).
- [163] J. Arndt, *Matters Computational – Ideas, Algorithms, Source Code* (Springer-Verlag, Berlin Heidelberg, 2011).
- [164] T. Prosen, Ergodic properties of a generic nonintegrable quantum many-body system in the thermodynamic limit, *Phys. Rev. E* **60**, 3949 (1999).
- [165] T. L. M. Lezama, S. Bera, and J. H. Bardarson, Apparent slow dynamics in the ergodic phase of a driven many-body localized system without extensive conserved quantities, *Phys. Rev. B* **99**, 161106 (2019).

SUPPLEMENTARY MATERIAL

Details of the POLFED algorithm with the geometric sum filtering

To find eigenvectors $|\psi_n\rangle$ and the corresponding eigenphases $e^{i\phi_n}$ of the unitary operator U_{KIM} , we employ the POLFED algorithm [62]. The algorithm is based on a block Lanczos iteration [155–157] performed for a polynomial $g_K(U_{\text{KIM}})$ of order K of the matrix U_{KIM} (see [158–161] for similar techniques). The matrix $g_K(U_{\text{KIM}})$ has the same eigenvectors $|\psi_n\rangle$ as U_{KIM} , but its eigenvalues are equal to $g_K(e^{i\phi_n})$. The idea of the approach is to use the polynomial g_K as a *spectral filter* so that its absolute value has a possibly sharp maximum for an argument $e^{i\phi_{\text{tg}}}$ (where ϕ_{tg} is a target eigenphase) at the unit circle on the complex plane. In that way, the eigenvectors $|\psi_n\rangle$ with ϕ_n close to ϕ_{tg} become eigenvectors of $g_K(U_{\text{KIM}})$ to eigenvalues with dominant absolute values. This enables the Lanczos iteration to quickly converge to those eigenvectors. A polynomial which can be effectively used as the spectral filter for unitary operators was proposed in [108], and is simply a geometric sum:

$$g_K(U_{\text{KIM}}) = \sum_{m=0}^K e^{-im\phi_{\text{tg}}} U_{\text{KIM}}^m. \quad (\text{S3})$$

The order of the polynomial K is fixed by the number of requested eigenvectors N_{ev} and the Hilbert space dimension $\mathcal{N} = 2^L$ as

$$K = f \frac{\mathcal{N}}{N_{\text{ev}}} \quad (\text{S4})$$

where the factor $f = 1.46$ was obtained from an optimization of the performance of the algorithm. For that choice, the algorithm converges to approximately N_{ev} eigenvectors after αN_{ev} steps of the Lanczos iteration, where $\alpha \approx 2.1$. Each step of the Lanczos iteration involves a single multiplication of a vector by the polynomial $g_K(U_{\text{KIM}})$ which reduces to K multiplications of the vector by U_{KIM} and basic linear algebra operations. Thus, the total computation cost is proportional to $\alpha N_{\text{ev}} KV + R$ where R is the cost of reorthogonalization of the vectors during the Lanczos iteration and V is the cost of the single matrix vector multiplication. The reorthogonalization costs scales as $R \sim N_{\text{ev}}^2 \mathcal{N}$. Since $V \sim L \mathcal{N}$ for U_{KIM} (as we argue below), the contribution $\alpha N_{\text{ev}} KV = \alpha f L \mathcal{N}^2$ dominates the total computation time. Notably, this contribution is independent of the number of requested eigenvalues N_{ev} . Hence, we can increase N_{ev} without a significant increase in the total computation time up to a point at which the reorthogonalization cost R starts to be comparable with $\alpha f L \mathcal{N}^2$. This, together with considerations about memory usage (which is proportional to $N_{\text{ev}} \mathcal{N}$) lead us to consider $N_{\text{ev}} = \min\{2^L/10, 1000\}$.

Once the Lanczos iteration for $g_K(U_{\text{KIM}})$ converges to vectors $|u_i\rangle$, we calculate the residual norms $\epsilon_i = ||U_{\text{KIM}}|u_i\rangle - \langle u_i|U_{\text{KIM}}|u_i\rangle u_i||$. Even though the order K of the polynomial (S3) may reach few thousands for the largest considered system sizes, we find consistently that the algorithm calculates the eigenvectors of U_{KIM} with a high numerical accuracy and the residual error norm $\epsilon_i < 10^{-14}$. Also, the algorithm calculate eigenvectors to all consecutive eigenphases in the vicinity of the target eigenphase $\phi_{\text{tg}} = 0$ so that the gap ratios r_n (which are determined by three consecutive eigenphases) can be calculated without problems.

The computation time of the POLFED algorithm is dominated by the multiple multiplications of vectors by the matrix U_{KIM} . To perform a single matrix vector multiplication we note that

$$U_{\text{KIM}} = e^{-ig \sum_{j=1}^L \sigma_j^x} e^{-i \sum_{j=1}^L (J \sigma_j^z \sigma_{j+1}^z + h_j \sigma_j^z)} \quad (\text{S5})$$

is composed of two operators, the first diagonal in the eigenbasis of σ_j^z (the Z basis) and the second diagonal in the eigenbasis of σ_j^x (the X basis). Thus, in order to calculate $U_{\text{KIM}} |\psi\rangle$, we start by expressing $|\psi\rangle$ in the Z basis, and multiply it by $e^{-i \sum_{j=1}^L (J \sigma_j^z \sigma_{j+1}^z + h_j \sigma_j^z)}$ which requires only $\mathcal{O}(\mathcal{N})$ operations. Subsequently, we transform the vector to the X basis, multiply it by the operator $e^{-ig \sum_{j=1}^L \sigma_j^x}$ diagonal in X basis, and finally we transform the vector back to the Z basis. To transform the vector between the bases, we employ a fast Hadamard transform [162, 163] which requires $\mathcal{O}(\mathcal{N} \log \mathcal{N})$ operations. The described procedure of multiplication by U_{KIM} is central for the efficiency of the POLFED approach described here, and also simplifies investigations of quantum dynamics in Floquet models [164, 165].

Ergodic-MBL crossover in KIM

A complete set of data for the average gap ratio \bar{r} , used in the determination of disorder strengths $W_{\bar{r}}^T(L)$ and $W_{\bar{r}}^*(L)$, is shown in Fig. S3(a). For KIM defined on chain of length $L \geq 6$, we observe a crossover between the ergodic regime $\bar{r} \approx r_{\text{COE}} \approx 0.53$ and MBL regime with $\bar{r} = \bar{r}_{\text{PS}} \approx 0.386$, which is a value for Poissonian level statistics that emerges due to the presence of local integrals of motion in the system.

The ergodic-MBL crossover looks qualitatively similar from the perspective of the rescaled entanglement entropy $\bar{s} = \bar{S}/S_{\text{COE}}$ which changes from 1 to 0 between the ergodic and MBL regimes, see Fig. S3(b). In the ergodic regime the average entanglement entropy \bar{S} is well approximated by the entanglement entropy S_{COE} of eigenstates of COE, shown in the inset in Fig. S3(b). The entanglement entropy S_{COE} increases according to a volume-law, i.e. proportionally to system size L . Linear fits yield $S_{\text{COE}} = aL + b$ with: $a=0.350$ ($a=0.347$) and

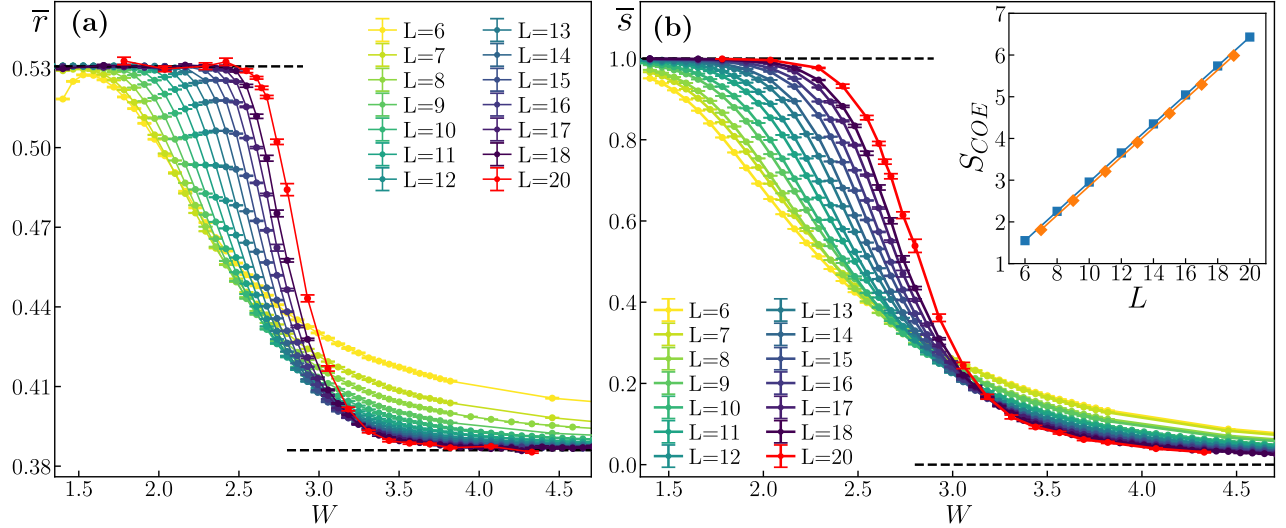


Figure S3. The average gap ratio \bar{r} (a) and the rescaled entanglement entropy \bar{s} (b) as functions of disorder strength W for Kicked Ising model (KIM) of system size L . The inset in (b) shows the average entanglement entropy S_{COE} of eigenstates of COE as function of L .

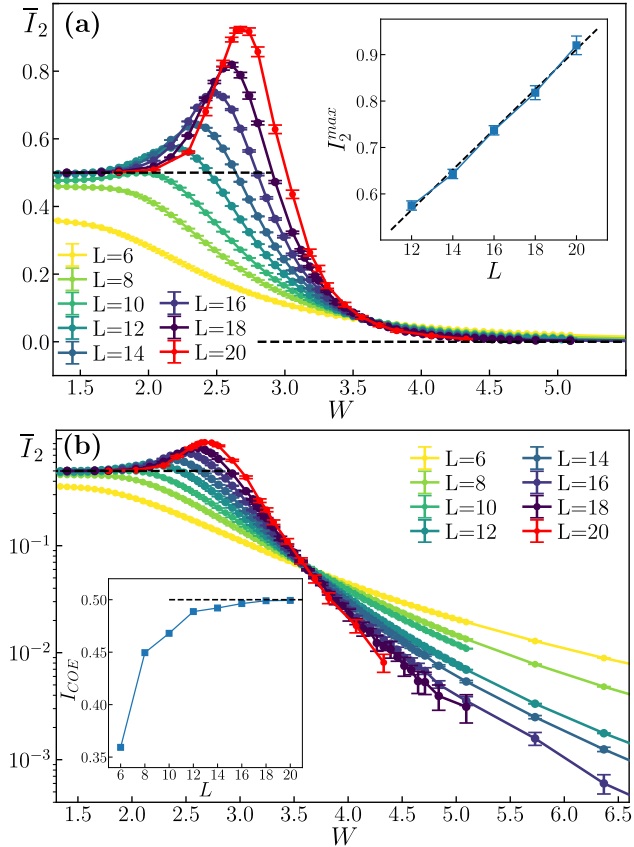


Figure S4. The average quantum mutual information (QMI) \bar{I}_2 as function of disorder strength W for KIM of system size L ; panel (a) - linear vertical scale, panel (b) - logarithmic vertical scale. The inset in (a) shows \bar{I}_2^{max} , the maximum of \bar{I}_2 , as a function of system size L . The inset in (b) shows the average QMI I_{COE} of eigenstates of COE as function of L .

$b=-0.551$ ($b=-0.509$) for even system sizes $L=6, 8, 10, 12$ ($L=14, 16, 18, 20$) and $a=0.349$ ($a=0.347$) and $b=-0.634$ ($b=-0.603$) for system sizes $L=7, 9, 11, 13$ ($L=15, 17, 19$) showing that the coefficient a approaches the expected value $\ln(2)/2 \approx 0.34657$ with increasing system size [119].

The average QMI \bar{I}_2 , shown as a function of disorder strength W in Fig. S4, admits a maximum at disorder strength $W_{\bar{i}_2}^m(L)$ for system size L . The value \bar{I}_2^{max} of the average QMI at the maximum is shown in the inset in Fig. S4(a) as a function of L . We observe that \bar{I}_2^{max} scales approximately linearly with the system size L . The inset in Fig. S4(b) shows that the average QMI of COE eigenstates, I_{COE} , saturates with the increase of L to a system size independent value $I_{COE} \approx 0.5$. As Fig. S4(b) shows, the average QMI \bar{I}_2 decreases approximately exponentially with disorder W as well as with the system size L in the MBL regime.

The behavior of the Schmidt gap $\bar{\Delta}$ and spin stiffness \bar{C} across the ergodic-MBL crossover is shown in Fig. S5. In contrast to \bar{r} , \bar{s} and \bar{i}_2 , the Schmidt gap and spin stiffness decrease monotonically with increasing system size (consequently, there are no crossing points that could be used to perform an analysis with disorder strength $W_X^*(L)$ for those quantities). The rate of the decrease is, however, markedly different in the ergodic and MBL regimes. In the former, $\bar{\Delta}$ and \bar{C} decrease approximately exponentially with system size L (as demonstrated by the insets in Fig. S5). In the latter regime, the decrease of the Schmidt gap and spin stiffness with L is much slower and at $W \gtrsim 4$, $L \geq 10$ the value of $\bar{\Delta}$ and \bar{C} appears to be independent, within the estimated error bars, of the system size L , consistently with the prediction that at $W \geq W_\infty \approx 4$ the KIM is in the MBL phase.

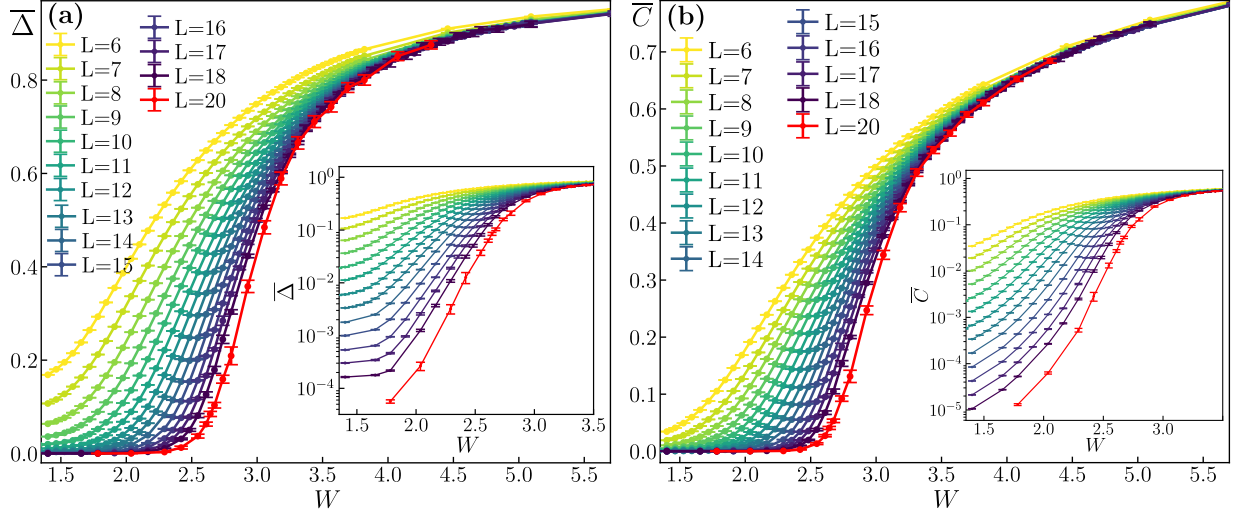


Figure S5. The average Schmidt gap $\bar{\Delta}$ (a) and spin stiffness \bar{C} (b) as functions of disorder strength W for KIM of system size L . The insets show the same, but using a logarithmic vertical axis.

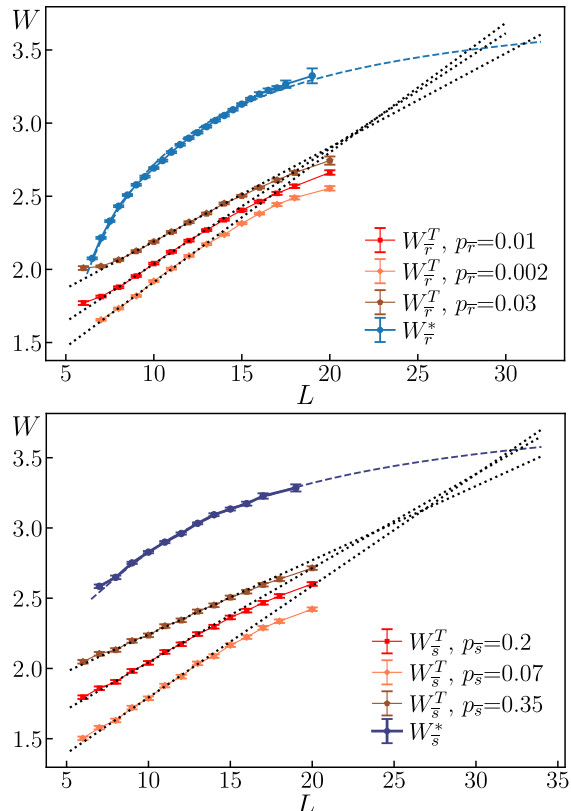


Figure S6. The disorder strength $W_X^T(L)$ for various choices of the threshold p_X compared with the crossing point $W_X^*(L)$. Panel (a) shows results for the average gap ratio $X = \bar{r}$, panel (b) presents results for the rescaled entanglement entropy $X = \bar{s}$. The dashed lines show an extrapolation of $W_X^*(L)$ with a second order polynomial in $1/L$, whereas the dotted lines denote first order polynomial in L fits in the regime of linear growth of $W_X^T(L)$.

The robustness of scaling of $W_X^T(L)$ with system size

In this section we analyze the robustness of the system size dependence of the disorder strength $W_X^T(L)$ at which the quantity X deviates from its ergodic value by a small parameter p_X . Fig. S6 shows $W_X^T(L)$ for various choices of p_X for the gap ratio $X = \bar{r}$ and for the rescaled entanglement entropy $X = \bar{s}$.

In Fig. S6(a) we observe a regime of linear increase of $W_{\bar{r}}^T(L)$ for $7 \leq L \leq 14$ and a deviation from this linear scaling at $L \geq 15$ for the considered values of $p_{\bar{r}} \in [0.002, 0.03]$. This confirms that the conclusions about system size scaling of $W_{\bar{r}}^T(L)$ reported in the main text are robust with respect to changes of $p_{\bar{r}}$. The length scale L_0^{KIM} is mildly dependent on $p_{\bar{r}}$, and it does not exceed 30 lattice sites for the considered interval of $p_{\bar{r}}$.

Analysis of the rescaled entanglement entropy yields $W_{\bar{s}}^T(L)$ shown in Fig. S6(b). The conclusions are the same as for $W_{\bar{r}}^T(L)$. There is a regime of a linear increase of $W_{\bar{s}}^T(L)$ with L for $6 \leq L \leq 14$ which is replaced by a sub-linear growth of $W_{\bar{s}}^T(L)$ for $L \geq 15$ (consistently with the presence of MBL transition at sufficiently large W). For $0.07 \leq p_{\bar{s}} \leq 0.2$, we observe that an extrapolation of $W_{\bar{s}}^T(L)$ yields $\tilde{L}_0^{\text{KIM}} \approx 32$ which is close to the length scale L_0^{KIM} obtained from the extrapolation of the linear scaling of $W_{\bar{r}}^T(L)$.

Additional data for finite size scaling analysis

In this section we provide additional data for the finite size scaling analysis at the ergodic-MBL crossover in KIM. Fig. S7(a) shows the cost function $\mathcal{F}_{\bar{s}}$ for the collapse of rescaled entanglement entropy \bar{s} . The conclusions are similar as for the gap ratio collapses reported in the main text. At sufficiently large system

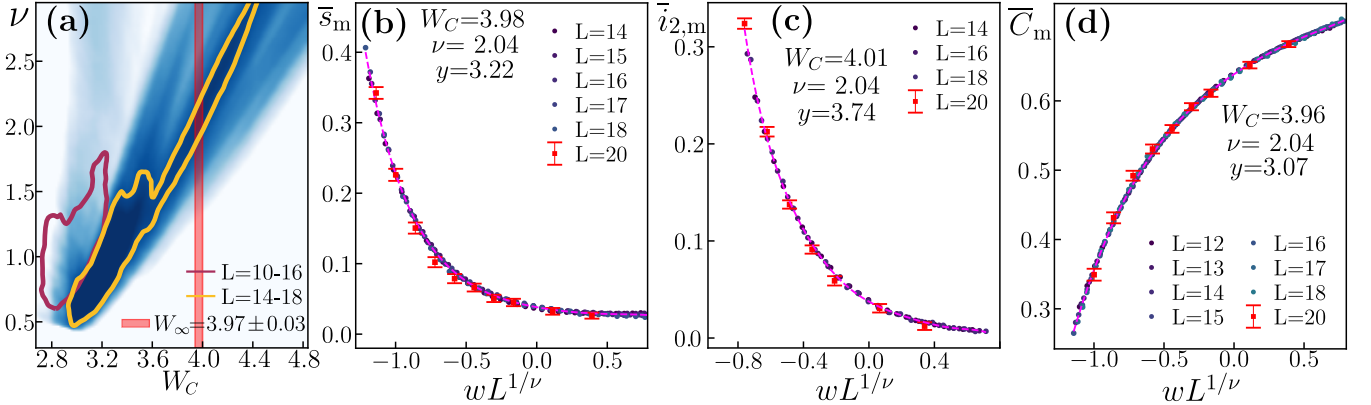


Figure S7. Supplementary data for finite size scaling analysis of ergodic-MBL crossover in KIM. Cost function $\mathcal{F}_{\bar{s}}$ for the collapse of the rescaled entanglement entropy \bar{s} is color coded for fixed ν , W_C in panel (a) (system sizes considered in the collapse $L = 14-18$). The contours highlight the change in the cost function system size by encompassing region of ν and W_C for which $\mathcal{F}_{\bar{s}} < 2\mathcal{F}_{\bar{s}}^{\min}$ where $\mathcal{F}_{\bar{s}}^{\min}$ is the minimum of $\mathcal{F}_{\bar{s}}$. Collapses for the rescaled entanglement entropy \bar{s}_m , rescaled QMI $\bar{i}_{2,m}$ and spin stiffness \bar{C}_m shown in (b), (c), (c); $w = (W - W_C)/W_C$ is the dimensionless distance from the critical point and the plots show the quantities with subtracted sub-leading correction to the scaling $X_m \equiv X - L^{-y}\psi_1(wL^{1/\nu})$.

sizes ($L = 14 - 18$), there appears a wide minimum of the cost function. This minimum is consistent with a broad interval of critical disorder strength W_C and exponent ν . Assuming, additionally, that $W_C \approx W_\infty \approx 4$, one obtains the power-law exponent $\nu \approx 2$ that is consistent with the Harris criterion for 1D disordered systems. The corresponding collapse of the data for the rescaled entanglement entropy is shown in Fig. S7(b). Collapses

for $\nu \approx 2$ and $W_C \approx 4$ for the rescaled QMI \bar{i}_2 and for the spin stiffness \bar{C} are shown in Fig. S7(c) and (d). Interestingly, the collapse of the gap ratio \bar{r} shown in the main text predicts that \bar{r}_m is equal to $\bar{r}_{PS} \approx 0.386$ characteristic for a localized system at the critical point $W = W_C$. At the same time, the values of \bar{s}_m and $\bar{i}_{2,m}$ seem to be not vanishing at $W = W_C$ despite being significantly smaller than their respective ergodic values.